

A&A manuscript no.

(will be inserted by hand later)

Your thesaurus codes are:

02 (11.01.2 11.03.1 12.04.2 13.25.2 13.25.3)

ASTRONOMY
AND
ASTROPHYSICS
17.1.2018

A Large-Area Cross-Correlation Study of High Galactic Latitude Soft and Hard X-ray Skies

Takamitsu Miyaji¹, Günther Hasinger², Roland Egger¹, Joachim Trümper¹, and Michael J. Freyberg¹

¹ Max-Planck-Institut für extraterrestrische Physik, D-85740 Garching b. München, Germany

² Astrophysikalisches Institut, An der Sternwarte 16, D-14482 Potsdam, Germany

Received date; accepted date

Abstract. We have made cross-correlation analyses of (2 – 15 keV) *HEAO-1* A2 and 1 keV *ROSAT* PSPC All-Sky Survey maps over a selected area ($\sim 4000 \text{ deg}^2$) with high galactic latitude ($b \gtrsim 40^\circ$). We have calculated the correlations for the bright *ROSAT* sources and residual background separately with the *HEAO-1* A2 TOT (2 – 10 keV) and HRD (5 – 15 keV) maps. In any case, the angular dependence of the cross-correlation function (CCF) was consistent with expected from the *HEAO-1* A2 collimator response function and the smoothing function of the *ROSAT* 1 keV map. The amplitude of the bright *ROSAT* source – A2 CCFs are consistent with expectations from model populations of AGNs and clusters of galaxies, which emit in both bands. However, the residual *ROSAT* background – A2 CCFs amplitude at zero degree are about a factor of three larger than that expected from the model populations.

Our soft-hard zero-lag and angular CCF results have been compared with the 1 keV auto-correlation function (ACF) found by Soltan et al. (1995) for the same *ROSAT* data. Their significant angular CCF at a scale of $\theta \lesssim 5^\circ$ is of an unknown origin and it could represent a new class of cosmic X-ray sources. If this 1 keV ACF has a hot plasma spectrum with $kT \sim 2 \text{ keV}$, contribution of this component is consistent with both our zero-lag CCF in excess of the population synthesis model prediction and the upper-limit to the angular CCF at $\theta \sim 2.5^\circ$. On the other hand, if this component has a lower temperature or a steeper spectrum, a major modification to the population synthesis model and/or an introduction of new classes would be needed.

Key words: Galaxies: active – Galaxies: clusters: general — (*Cosmology*): Diffuse Radiation — X-rays: galaxies – X-rays: general

1. Introduction

With deep *ROSAT* observations of blank fields, up to $\sim 60\%$ of the soft ($\lesssim 2 \text{ keV}$) cosmic X-ray background (XRB) has been resolved into individual sources (e.g. Hasinger et al. 1993). A number of groups have worked/are currently working on identification programs of these *ROSAT* sources and we can expect that we will have the overall picture of the origin of most of the soft ($\sim 1 \text{ keV}$) X-ray background including contributing source populations and their cosmological evolution. With *ASCA* observations of blank fields, the XRB at higher energies (2 – 10 keV) have also been resolved into sources, although the resolved fraction of the total XRB flux is smaller than that of *ROSAT* because of the limited spatial resolution. While these observational efforts are rapidly in progress, the unified theory of AGNs and supporting X-ray observations of AGNs for the basic framework of the unified scheme have provided insights to the origin of the bulk properties of the XRB. In particular, intrinsic photoelectric absorption observed in the X-ray spectra of Seyfert 2 galaxies (e.g. Awaki et al. 1991; Mulchaey et al. 1992), consistent with the view of the unified scheme that a Seyfert 2 galaxy is a Seyfert 1 seen at an angle where a torus surrounding the central engine blocks the line of sight. A wide range of absorption column densities have been observed (Schartel et al. 1995) for a hard X-ray flux-limited sample of AGNs by Piccinotti et al. (1982). Models of the XRB with evolving populations of unabsorbed and internally-absorbed AGNs with various absorption column densities, based on the unified scheme of AGNs have been successfully made consistent with many observational properties of the XRB (Madau et al. 1994; Comastri et al. 1995). In particular, they explained the global spectral shape of the XRB, especially the characteristic break at 30 keV and source counts in soft and hard X-rays. While these models are basically successful, there is still room for major modifications, given current observations. A recent *ASCA* observation of NGC 3628 by Yaqoob et al. (1995) showed that the X-ray ($E \lesssim 10 \text{ keV}$) spectrum of this spiral galaxy, which

had previously been classified as a starburst, is rather flat. Based on this observation, they argued that the contribution of low-luminosity extragalactic X-ray sources, like NGC 3628, to the $E \gtrsim 2$ keV XRB could be significant. Such a low X-ray luminosity population has been deliberately neglected in the Madau et al. (1994) and Comastri et al. (1995) models. Also these models assumed a simple version of the AGN unified scheme where the ratio of the numbers of absorbed and unabsorbed objects does not depend on their intrinsic X-ray luminosity. However, Barcons et al. (1995) argued that this is not likely to be the case but rather the fraction of the unabsorbed AGNs (type 1) should increase with the intrinsic luminosity.

Besides detailed studies of the nature of individual X-ray sources which can contribute to the XRB, statistical properties of the spatial fluctuation of the unresolved background provide us with other perspectives of cosmic X-ray sources. Fluctuations of the unresolved XRB have been used to infer the $\log N - \log S$ relation below the source detection flux-limit (e.g. Shafer 1983; Hasinger et al. 1993; Barcons et al. 1994). The angular auto-correlation function is often used to describe spatial structure of the XRB. Many authors discussed the constraints on the combination of the X-ray volume emissivity and clustering properties of the X-ray sources from the ACF (or upper limits of ACF) (e.g. Danese et al. 1993; Carrera et al. 1991; Soltan & Hasinger 1994). While the XRB ACF traces the properties of all the X-ray sources along the line of sight and thus the interpretation is highly model dependent, cross-correlating catalogs of known sources with the XRB gives more concrete information on the XRB constituents. In particular, cross-correlation functions (CCF) of unresolved XRB spatial fluctuations with galaxy catalogs give information on the contribution of these galaxies and objects clustered with these sources to the XRB (Jahoda et al. 1991, 1992; Lahav et al. 1993; Miyaji et al. 1994; Roche et al. 1994; Barcons et al. 1995).

Auto and cross-correlation function analyses over a large region of the sky occasionally discover new components of cosmic X-ray emission. The auto-correlation of the *HEAO-1* A2 hard X-ray map nearly over the whole sky at high galactic latitudes revealed a weak large-scale component at $\theta \lesssim 40^\circ$, which perhaps is associated with structures in the supergalactic plane (Jahoda 1993). Using the *ROSAT* All-Sky Survey (RASS) data, Soltan et al. (1995) found an extragalactic extended component in the ACF of at 1 keV at a scale of 5 degrees. They also found an angular correlation at 5 – 10 degree scales in the CCF between the 1 keV XRB and the positions of the Abell clusters. They modeled the latter component as a 10 Mpc scale diffuse gas surrounding clusters of galaxies, which itself had not been recognized in any previous observation. They found, however, that clusters of galaxies, considering this putative circum-cluster emission and clustering of clusters, explain only about a third of their extended 1 keV

ACF component. Thus the main portion of the extended ACF could represent still a new population of cosmic X-ray emission and investigating their nature is only possible by statistical analyses over a large region of the sky.

In this paper, we present the results and possible interpretations of a cross-correlation analysis between the soft (~ 1 keV) X-ray sky observed with *ROSAT* PSPC All-Sky Survey and the hard (2 – 15 keV) X-ray sky observed with the *HEAO-1* A2 experiment. The purpose of the correlation between soft-hard X-rays presented in this paper is two-folded. Zero-lag and angular cross-correlation functions (CCFs) between surface brightnesses contain information on X-ray sources common to these two bands. Thus this would give additional constraints to the population synthesis models. Especially, it would give a check to the models based on unabsorbed and absorbed AGNs. A large area correlation study also may give a clue to the nature of the extended ACF component that Soltan et al. (1995) found. The scope of this paper is as follows: In Sect.2, we explain the data used. We explain the CCF calculation and present the results of the calculation in Sect.3. Sect.4 presents formulations relating observed CCF with models including individual sources in the population synthesis models and extended components. In Sect.5, we use the formulation to compare various models with the observations. The purpose of the section is to check the effects of various components on the observed CCF and we do not intend to construct a complete model consistent with all the existing constraints. Such an elaborate modeling would be a topic of a future paper. Finally we conclude our discussion in Sect.6.

2. Data

2.1. The *ROSAT* All-Sky Map

We have used a clean surface brightness map constructed from the *ROSAT* (Trümper 1983) PSPC (Pfeffermann et al. 1986) All-Sky Survey (Snowden & Schmitt 1990; Voges 1992) in the north galactic pole region. In making the map, the period of Short-Term Enhancements has been excluded and non-cosmic backgrounds (particle background, solar scattered X-rays and the Long-Term Enhancements) have been subtracted as explained in Snowden et al. (1995). Soltan et al. (1995) selected a relatively large portion of the high galactic latitude sky which is free from contamination by galactic structures to investigate the extragalactic structures in the soft X-ray sky:

$$70^\circ < l < 250^\circ, \quad b > 40^\circ. \quad (1)$$

We also use this area for our correlation with the hard X-ray sky. We also included a 3.5 degree wide strip surrounding this region in our analysis, taking the larger *HEAO-1* A2 collimator response function into account. In this work, we have only used the map in the R6 (PI channel range

91 – 131, corresponding to 0.9 – 1.3 keV band (Snowden et al. 1993), which is least contaminated by the galactic emission, scattered solar X-rays, and particle background. The energy response curve of the R6 band is shown as a solid line in Fig. 1.

The conversion factor between the observed R6 count rate and the 0.5 – 2 keV flux before the absorption by the Galaxy is $3.24 \times 10^{-11} \text{ erg s}^{-1} \text{ cm}^{-2} / (\text{R6 cts s}^{-1})$ for a power-law photon index of ($\alpha_{ph} = 2.0$) for the absorption column density of $N_H = 1.8 \times 10^{20} \text{ cm}^{-2}$, which is the average galactic value for the region. The range of the galactic column in the region is $0.6 - 4. \times 10^{20} \text{ cm}^{-2}$ and the conversion factors in that region differ from the mean value by $\lesssim 5\%$. Therefore we use the average N_H value for the whole region for the analysis.

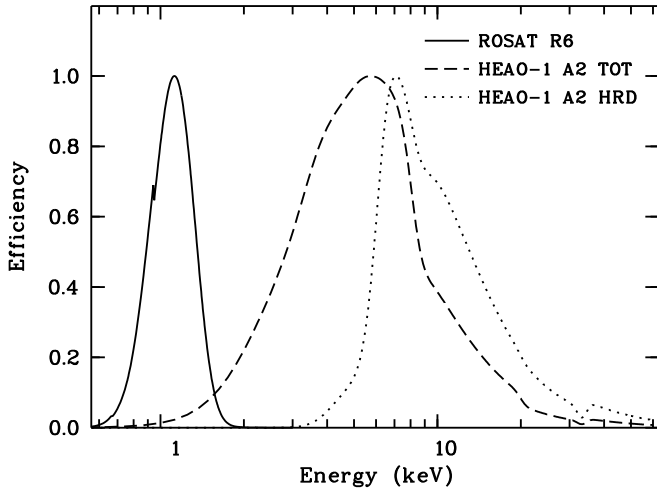


Fig. 1. Energy response curves of the *ROSAT* R6 and *HEAO-1* A2 TOT/HRD bands, used in our CCF analysis, are shown as labeled. Each curve is normalized at its peak

2.2. The *HEAO-1* A2 Hard X-ray Map

We have used the all-sky hard X-ray map constructed from the combination of the HED3 and MED detectors of the *HEAO-1* A2 experiment (Rothschild et al. 1979). The combination of the detectors is sensitive in 2–60 keV. Conventionally all-sky maps from this combination are analyzed in a number of standard colors defined as weighted sums of counts from certain combinations of detector layers and pulse height channels (discovery scalars; see Allen et al. 1994). In this work, we have used the *TOTAL* (indicated by TOT) and *HARD* (indicated by HRD) band maps. The energy response curves of the TOT and HRD bands are shown as dashed and dotted lines respectively in Fig. 1. For the cosmic X-ray background and canonical AGN spectrum, most of the photons come from the 2 – 10 keV range for the TOT map and 5 – 15 keV range for the

HRD map. For a power-law spectrum with photon index $\alpha_{ph} = 1.7$, the conversion factor between the TOT count rates and the 2–10 keV flux is $2.2 \times 10^{-11} \text{ erg s}^{-1} \text{ cm}^{-2} (\text{TOT cts s}^{-1})^{-1}$ and the conversion factor between the HRD count rates and the 5 – 15 keV flux is $1.8 \times 10^{-11} \text{ erg s}^{-1} \text{ cm}^{-2} (\text{HRD cts s}^{-1})^{-1}$. These conversion factors vary only by $\lesssim 4\%$ for a 40 keV bremsstrahlung spectrum, an $\alpha = 0.7$ power-law, the same power-law with neutral gas absorption up to $N_H \lesssim 10^{24} \text{ cm}^{-2}$.

The maps used here have the beam profile (or the collimator response function) well represented by (Shafer 1983):

$$B_{A2} = \max(1 - \frac{|x|}{3.0}, 0) \max(1 - \frac{|y|}{1.5}, 0) \quad (2)$$

where y represents the coordinate along the scan direction of the survey, which is along the great circle of a constant ecliptic longitude, and x is the coordinate along the direction perpendicular to the scan path.

2.3. Excluded Regions

Regions around conspicuous sources in the R6 band have been excluded from the analysis in order to avoid the situation that a few sources dominate the correlation signal. Those are the Coma cluster, Abell 1367, Mkn 421 and NGC 4253 (Mkn 766). These are all the sources in the region with R6 count rates greater than 0.9 counts per second. We have excluded 3.4° radius regions (corresponding to the maximum extent of the A2 beam) around Mkn 421 and NGC 4253. The exclusion radius around the two conspicuous galaxy clusters (i.e. the Coma cluster and Abell 1367) was 7° . In addition, we have also excluded the 3.4° degree radius regions around the *HEAO-1* A2 sources in Piccinotti et al. (1982). The flux cutoff of this complete flux-limited catalog is $1.25 \text{ counts s}^{-1}$ in the *HEAO-1* A2 R15 band, which is similar to the TOTAL band used here but a little harder (Allen et al. 1994).

3. The Soft-Hard Cross-Correlation Function

3.1. The CCF calculation

We have calculated the angular cross-correlation functions between the *ROSAT* All-Sky Survey R6 and *HEAO-1* A2 maps in the region defined in Eq.(1). Since the *ROSAT* All-Sky map has a much higher spatial resolution and denser samplings, we have smoothed the *ROSAT* data before correlating. As the smoothing function, we took the form represented by Eq. (2) but smaller FWHMs in order to improve the signal-to-noise ratio of the correlation. Among a number of sizes we tried for the smoothing function, the best results could be obtained when we chose 1.5° and 0.75° (FWHMs) in the x and y directions respectively.

As a statistical measure to indicate the degree of correlation between two maps (here we denote the two maps

by subscripts *s* and *h*, representing *soft* and *hard* respectively), we calculate the angular cross-correlation function (CCF):

$$W_{\text{sh}}(\theta) = \frac{N_{\text{pair}}^{-1} \sum_{ij} [(I_{si} - \langle I_s \rangle) (I_{hj} - \langle I_h \rangle)]}{\langle I_s \rangle \langle I_h \rangle}, \quad (3)$$

where I_s and I_h are the *ROSAT* and *HEAO-1* A2 intensities measured at the gridding points which are within the region defined above. We have taken pairs along the scan path (ecliptic longitude) to calculate the angular correlation in order to make use of the narrower collimator response.

The uncertainties of the correlation functions are estimated by correlating the *ROSAT* map with different parts of the sky in the *HEAO-1* A2 map. We made this by rotating the *ROSAT* map around the galactic pole and calculating the correlation with the A2 map in the same way. We have also transposed the *ROSAT* map about the galactic equator followed by rotations about the galactic pole to calculate the correlation with the A2 map. Thus we produced a number of different artificial null samples with equivalent statistical properties. Regions around Piccinotti et al. sources are excluded as we did in the real correlation calculation. We also excluded 20° and 25° regions around LMC and SMC respectively. We have rotated the map in steps of 30° on both hemispheres, thus we get 23 null-hypothesis CCFs between unrelated parts of the sky. These give a fair estimate of the uncertainties of the correlation function.

3.2. CCF of *ROSAT* bright sources with the *HEAO-1* A2 Maps

In order to evaluate the contribution to the CCF from bright *ROSAT* sources, we have made a list of bright sources by performing a source detection procedure to the R6 map in the region defined in Eq.(1). The source detection has been made to the map gridded in $12' \times 12'$ pixels, larger than the *ROSAT* PSPC point spread function, and thus is much less sensitive than the source detection procedure directly applied to the full-resolution *ROSAT* All-Sky Survey data. A *ROSAT* All-Sky Survey bright source list using such a procedure (Voges 1995) is in progress at the time of writing this paper. An analysis using the source list will be a topic of a future paper. In this work, we use the coarsely rebinned map to obtain a complete R6 flux-limited sample of bright sources. As described by Hasinger et al. (1993), the source detection have been made in two steps: the first step is to slide a detection cell over the map and find excess over the region immediately surrounding the cell (LDETECT). A background map was created by removing the sources detected in the LDETECT procedure, filling the holes by the mean counts surrounding them, and making a bi-cubic spline fit to the filled map. This procedure gives a more robust measure of the background for the source detection than taking the

background from immediate surroundings. Then we slid the detection cell again to the original map to find significant excess counts over the background map created in the above process (MDETECT).

The source detection have been made using procedures within the *EXSAS* software package (Zimmermann et al. 1994). The size of the detection cell has been taken to be 3×3 cells ($36' \times 36'$) and the source detection threshold is set at a significance of $-\log P_i = 10$, where P_i is the probability that the random Poisson fluctuation make the excess counts in the cell. This roughly corresponds to a 4σ excess of a Gaussian fluctuation. Since the *ROSAT* PSPC PSF and extents of clusters of galaxies (except for closest ones, which have been excluded from the analysis (Sect. 2.3) are much smaller than the size of the detection cell, the source list from the MDETECT procedure is expected to be free from significant biases.

In the least sensitive areas, the detection limit was 0.08 R6 cts s^{-1} . If we assume a Seyfert 1-like broken power-law spectrum with $\alpha_{ph} = 2.3$ for $E \leq 1.5$ keV, $\alpha_{ph} = 1.7$ for $E > 1.5$ keV, and the average galactic N_H of the region ($= 1.8 \times 10^{20} \text{ cm}^{-2}$), 0.08 R6 cts s^{-1} corresponds to a $0.5 - 2$ keV flux of $2.7 \times 10^{-12} \text{ erg cm}^{-2} \text{ s}^{-1}$ and $2 - 10$ keV flux of $3.8 \times 10^{-12} \text{ erg cm}^{-2} \text{ s}^{-1}$.

By this procedure, we have obtained a complete flux-limited ($> 0.08 \text{ R6 cts s}^{-1}$) sample of 183 sources above this limit over the 4575 deg^2 area of the sky ($0.04 \text{ sources deg}^{-2}$). The $\log N - \log S$ function of the detected sources has a Euclidean slope. The number density corresponds to that of the *Einstein* Medium Sensitivity Survey (EMSS) (Gioia et al. 1990) above $4.1 \times 10^{-12} \text{ erg cm}^{-2} \text{ s}^{-1}$ in $0.3 - 3.5$ keV. They are consistent if the $0.3 - 3.5$ keV flux versus R6 count rate conversion factor is $\sim 5 \times 10^{-11} \text{ erg s}^{-1} \text{ cm}^{-2} (\text{R6 cts s}^{-1})^{-1}$. For a power-law spectrum with $\alpha_{ph} = 2.0$, this factor is $\sim 5.7 \times 10^{-11} \text{ erg s}^{-1} \text{ cm}^{-2} (\text{R6 cts s}^{-1})^{-1}$ and for a $kT = 2$ keV Raymond-Smith spectrum (heavy element abundance=0.4 cosmic), this number is $\sim 4.4 \times 10^{-11} \text{ erg s}^{-1} \text{ cm}^{-2} (\text{R6 cts s}^{-1})^{-1}$. Thus our bright source counts are consistent with the EMSS counts considering a possible range of the source spectra.

We have calculated the CCF between the detected sources (R6 count rate weighted) and the *HEAO-1* A2 maps in the same way as Sect. 3.1. The errors of these CCFs have been calculated also in the same manner.

Using the detected sources, we have also constructed a *source-removed ROSAT* map. This has been made by replacing the 3×3 image pixel regions around the sources with R6 count rate greater than 0.08 cts s^{-1} by the pixel values in the same regions of the background map produced for the MDETECT procedure (see above). We have also calculated the CCF between the source-removed map and the *HEAO-1* A2 maps. The source-removed map still contains sources below the limit and we expect that such fainter sources still contribute to the correlation.

Table 1. The Zero-lag Correlation Results

Id.	R6 cr. range [cts s ⁻¹]	HEAO-1 A2 Band	$\langle I_s \rangle$ [cts s ⁻¹ deg ⁻²]	$\langle I_h \rangle$ [cts s ⁻¹ deg ⁻²]	$W_{sh}(0)$
T1	0 – 0.9	TOT	2.9×10^{-1}	7.2×10^{-1}	$(3.2 \pm 0.4) \times 10^{-3}$
T2	0 – 0.08	TOT	2.9×10^{-1}	7.2×10^{-1}	$(1.7 \pm 0.3) \times 10^{-3}$
T3	0.08 – 0.9	TOT	6.1×10^{-3} ^a	7.2×10^{-1}	$(6.6 \pm 1.0) \times 10^{-2}$
T4	0.2 – 0.9	TOT	2.6×10^{-3} ^a	7.2×10^{-1}	$(8.3 \pm 1.7) \times 10^{-2}$
H1	0 – 0.9	HRD	2.9×10^{-1}	8.6×10^{-1}	$(2.4 \pm 0.4) \times 10^{-3}$
H2	0 – 0.08	HRD	2.9×10^{-1}	8.6×10^{-1}	$(1.0 \pm 0.3) \times 10^{-3}$
H3	0.08 – 0.9	HRD	6.1×10^{-3} ^a	8.6×10^{-1}	$(5.4 \pm 1.6) \times 10^{-2}$
H4	0.2 – 0.9	HRD	2.6×10^{-3} ^a	8.6×10^{-1}	$(6.6 \pm 2.6) \times 10^{-2}$

^a Intensity from sources in the quoted flux range

3.3. Results of the CCF Calculations

Significant zero-lag correlation signals have been detected in most of the cases we have calculated ($\theta = 0$ case of Eq. [3]). Table 1 summarizes the zero-lag correlation results for the calculations we made for various cases. The second column of Table 1 is the R6 count rate range of the sources correlated with the A2 map. A zero value of the lower bound in this column means that the R6 surface brightness map has been used and a non-zero value represents that the source list in the quoted flux range explained in Sect. 3.2 has been used.

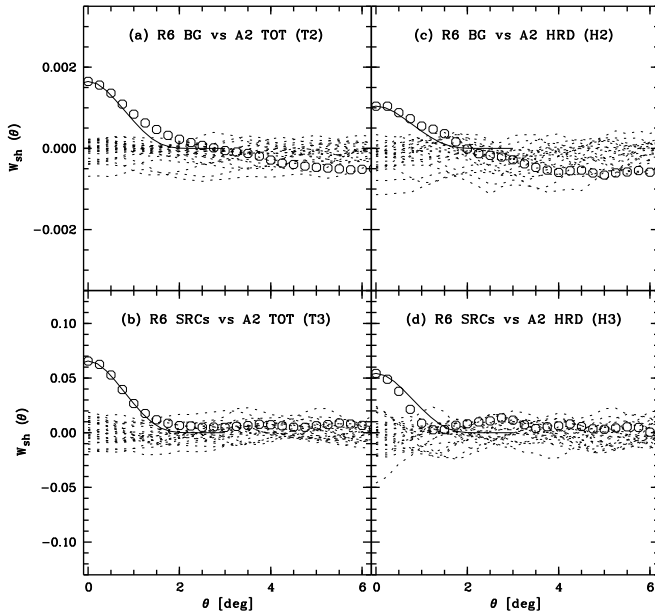


Fig. 2. The angular CCF for selected cases as labeled. The open octagons show the observed correlation and the dotted lines show the 23 uncorrelated cases. The solid line is the angular dependence of the Poisson effect caused by the A2 collimator response function and smoothing

The angular correlation functions for selected cases have been plotted in Fig. 2 along with the angular correlation functions between the rotated R6 maps with the A2 map to show the dispersion of the CCF when no real sky-correlation exists. The label in each figure corresponds to the correlation ID in Table 1. Also the angular dependence of the CCF in case of the purely Poissonian case (see Sect. 4) due to the A2 collimator response and the *ROSAT* All-Sky Survey map smoothing, normalized at $\theta = 0$, has been plotted on each plot. In any case, we did not find significant extended component in the angular CCF beyond expected from the Poisson effect.

4. Basic Formulations

The CCF depends on Poisson and clustering effects. The Poisson effect is caused by individual sources which emit both soft and hard X-rays and the angular dependence of the correlation coefficient simply reflects the overlap of the finite-sized beams of soft and hard X-ray observations and smoothings. The clustering effect reflects the real sky structure of the X-ray sources common to (or at least correlated with) both soft and hard X-rays. This structure may be due to clustering of sources or a diffuse X-ray component which extends to a scale comparable or larger than the size of the beam. If one is concerned with real extended structure, the distinction between Poisson and clustering effects is somewhat ambiguous. In our case, the extent of the X-ray emission from an individual galaxy cluster is much smaller than the beam size of the *HEAO-1* A2 experiment and thus we treat them in the Poisson term. On the other hand, we treat the effect of possible diffuse components with scales of several degrees in the clustering effect.

The observed angular correlation function is then, expressed by the sum of two terms (cf. Lahav et al. 1993; Miyaji 1994; Miyaji et al. 1994):

$$W_{sh}(\theta) \langle I_s \rangle \langle I_h \rangle = \eta_p(\theta) + \eta_c(\theta), \quad (4)$$

where $\mathcal{I}_{s,h}$ represent the intensities of soft and hard X-rays per *beam* respectively:

$$\mathcal{I}_{s,h} \equiv \int \langle I_{s,h} \rangle B_{s,h}(\hat{\Omega}) d\Omega \equiv \langle I_{s,h} \rangle \Omega_{Bs,h}, \quad (5)$$

where $\hat{\Omega}$ is the unit vector towards the solid angle element $d\Omega$.

As we will see in Sect. 5, the correlation is dominated by local sources and cosmological evolution is not important in our case, because of the large beam of the *HEAO-1* A2 experiment. However, we will develop a full cosmological formulation below for completeness.

4.1. Poisson Effect from Common Sources

We can express the Poisson term of the cross-correlation function as:

$$\eta_p(\theta) = \int \int S_s S_h N_{sh}(S_s, S_h) dS_s dS_h \times \langle \int B_s(\hat{\Omega}) B_h(\hat{\Omega} - \theta) d\Omega \rangle, \quad (6)$$

where $N_{sh}(S_s, S_h) dS_s dS_h$ is the *bivariate* $N(S)$ function defined as the number of sources per solid angle whose soft and hard X-ray fluxes fall in the ranges $[S_s - 0.5 dS_s, S_s + 0.5 dS_s]$ and $[S_h - 0.5 dS_h, S_h + 0.5 dS_h]$ respectively. Also θ is the offset vector between hard and soft X-ray measurements. The flux integrations (over S_s or S_h) are over source fluxes included in the corresponding maps. When we use a surface brightness map where bright sources above a certain limit are excluded, this limit defines the upper bound of the integration and the lower bound is zero. When we use a complete flux-limited source list, this flux limit defines the lower bound.

The double integral over the soft and hard fluxes in Eq. (6) can be calculated for given population synthesis models. Let us suppose we have evolving populations of objects with the bivariate soft-hard luminosity function (for the i -th population) per comoving volume: $\hat{\Phi}_i(L_s, L_h, z) dL_s dL_h$, where each population is assumed to have a universal spectral shape for simplicity. Then,

$$\int S_s S_h N(S_s, S_h) dS_s dS_h = \frac{c}{16\pi^2 H_0} \int_0^{z_{\max}} \times \frac{1}{D_L(z)^2 (1+z)^3 (1+\Omega_0 z)^{\frac{1}{2}}} \sum_{i=\text{pop}} [K_{si}(z) K_{hi}(z) \times \int_{L_s^{\min}}^{L_s^{\max}} \int_{L_h^{\min}}^{L_h^{\max}} L_s L_h \hat{\Phi}_i(L_s, L_h, z) dL_h dL_s] dz, \quad (7)$$

where $D_L(z)$ is the luminosity distance as a function of redshift and $K_{s(h)i}$ is the soft (hard) band K-correction for the i -th population. The luminosity integrations are over luminosities where the observed flux falls in the range of source fluxes included in the corresponding correlating

maps. Thus the bounds of the luminosity integrations depend on redshift and the spectrum of the population. Now let the soft and hard X-ray luminosities of each population be related by $L_s = a_i L_h$. Then the double integral over hard and soft X-ray luminosities can be reduced to:

$$\int_{L_s^{\min}}^{L_s^{\max}} \int_{L_h^{\min}}^{L_h^{\max}} L_s L_h \hat{\Phi}_i(L_s, L_h, z) dL_h dL_s = \int_{\max(L_s^{\min}, a_i L_h^{\min})}^{\min(L_s^{\max}, a_i L_h^{\max})} a_i L_s^2 \hat{\Phi}_i(L_s, z) dL_s, \quad (8)$$

where $\hat{\Phi}_i(L_s, z)$ is the comoving soft X-ray luminosity function, which we can find in literature based on *ROSAT* surveys (e.g. Boyle et al. 1993, 1994). In the case of the pure-luminosity evolution of the power-law form, $L(z) = L(0)(1+z)^p$, the evolving luminosity function can be expressed by the present epoch one:

$$\hat{\Phi}_{si}(L_s, z) = \hat{\Phi}_{si}([1+z]^{-p} L_s, 0) (1+z)^{-p}. \quad (9)$$

4.2. Extended Component

The underlying angular CCF of the soft and hard X-ray skies

$$w_{sh}(\theta) \equiv \frac{\langle I_s(\hat{\Omega}) I_h(\hat{\Omega} + \theta) \rangle}{\langle I_s \rangle \langle I_h \rangle} - 1, \quad \theta > 0 \quad (10)$$

reflects the extended structure common to soft and hard X-rays and clustering of X-ray sources.

The *observed* angular correlation function ($W_{sh}(\theta)$) is contributed by the underlying angular cross-correlation function $w_{sh}(\theta)$ of the real sky. The term η_c in Eq. 4 reflects this component:

$$\eta_c(\theta) = \langle I_s \rangle \langle I_h \rangle \times \int \int w_{sh}(\theta') B_s(\hat{\Omega}_1) B_h(\hat{\Omega}_2 - \theta) d\Omega_1 d\Omega_2, \quad (11)$$

where $\theta' = |\hat{\Omega}_1 - \hat{\Omega}_2 + \theta|$. In effect, the underlying angular correlation function is smoothed with the convolution of soft and hard beams. At large separations (θ is much larger than the scale size of the beam), $W_{sh}(\theta) \approx w_{sh}(\theta)$ and the Poisson term is zero.

The underlying w_{sh} can be expressed by the cosmologically evolving soft and hard volume emissivities and the spatial correlation function of soft and hard X-ray sources. The expression is quite parallel to the case of ACF found in literature (e.g. Danese et al. 1993; Soltan & Hasinger 1994). Let us consider populations of soft and hard X-ray emitting sources with redshift dependent comoving volume emissivities of $\hat{\rho}_s(z)$ and $\hat{\rho}_h(z)$. Let the spatial correlation function between these populations be $\xi_{sh}(r, z)$. Then, in the small-angle long-distance approximation,

$$w_{sh}(\theta) = \frac{c}{16\pi^2 H_0} \int \hat{\rho}_s(z) K_s(z) \hat{\rho}_h(z) K_h(z) \times \int \xi_{sh}(\sqrt{(D_A \theta)^2 + x^2}, z) dx (1+z)^{-4} (1+\Omega_0 z)^{\frac{1}{2}} dz, \quad (12)$$

where $K_s(z)$ and $K_h(z)$ are the K-corrections for the soft and hard X-ray bands respectively and $D_A(z)$ ($= D_L(z)(1+z)^{-2}$) is the angular distance.

5. Comparison of Models with Observations

5.1. AGN and Cluster Contributions

We have calculated the expected contributions from two major classes of extragalactic X-ray sources, i.e. AGNs and clusters of galaxies, to the observed zero-lag correlation strengths using the population synthesis technique. For the following models, the standard cosmology with $\Lambda = 0$ and $q_0 = 0$ has been used. We also denote the Hubble constant by $H_0 = 50h_{50}\text{km s}^{-1}\text{Mpc}^{-1}$. Note that the expected correlations from the models do not depend on the value of the Hubble constant.

As the first model (Model P1, where P represents the Poisson effect) we have constructed an AGN population synthesis model following the recipe by Comastri et al. (1995) for their baseline model. Contributions from X-ray clusters of galaxies have been added. In adding the cluster contribution, we have used the analytical forms of the 2 – 10 keV X-ray luminosity function (XLF) by Edge et al. (1990). We have used their volume-limited expression for $z < 0.1$ and flux-limited expression for $0.1 \leq z < 0.17$, taking into account the deficit of most luminous clusters at higher redshifts they observed. In the $0.17 \leq z < 0.6$, we have used the power-law forms of the XLF given by Henry et al. (1992) in their three redshift bins. They showed the steepening of the XLF for higher redshift bins. Thus their power-law form would predict too large an XLF at low X-ray luminosities (below their sample limit). Thus we take the smaller (in comoving coordinates) of the Edge et al. analytical form and the Henry et al. power-law form. We have taken the 2–10 keV X-ray luminosity range of $0.01 \leq L_{x44} \leq 120$, where L_{x44} represents X-ray luminosity measured in units of $10^{44}h_{50}^{-2}\text{erg s}^{-1}$. The clusters have been assumed to have X-ray spectra represented by the Raymond & Smith plasma with a heavy element abundance of 0.4. The temperatures of a cluster have been chosen from $kT = 1, 1.5, 2.5, 4, 7, 10$ keV, according to its luminosity between the minimum and the maximum values given above. The dividing luminosities are $L_{x44} = 0.02, 0.1, 0.5, 3.0$, and 15.0, which roughly corresponds to the X-ray luminosity versus temperature correlation (David et al. 1993). There is a significant scatter in the luminosity – temperature correlation but this has not been taken into account in the model. However, the results are insensitive to the detailed assumption on this $L_x - T$ correlation. For example, assuming a single temperature of $kT = 4$ keV for all clusters changed the result by 10% for T2, which is somewhat smaller than the statistical error of the observation. The expected correlation from this model is compared with data in Table 2. We compare the values of $W_{\text{sh}}(0)\langle I_s \rangle \langle I_h \rangle$

because this quantity is proportional to the contribution from each of the R6 sources at a certain flux-range and source-removed background.

Table 2. Comparison of correlation results with models

Id.	$W_{\text{sh}}(0)\langle I_s \rangle \langle I_h \rangle$ [10^{-4} R6 cts s^{-1} A2 cts s^{-1}]					
	Observed	Models ^a				
		P1	P2	P3	E1	E2
T2	3.5 ± 0.6	0.9	1.3	0.9	3.1	1.9
T3	2.9 ± 0.4	2.5	3.6	2.5
H2	2.5 ± 0.7	0.7	1.1	0.8	0.8	0.2
H3	2.8 ± 0.8	1.7	2.5	1.7

^a See Sect. 5.1 for the explanation of model P1, Sect. 5.3 for P2 & P3, and Sect. 5.5 for E1 & E2

Figure 3 shows the cumulative contributions of clusters, type 1 AGNs and type 2 AGNs in model P1 to the $W_{\text{sh}}(0)\langle I_s \rangle \langle I_h \rangle$ values for selected correlations. The observed value with $\pm 1\sigma$ range is shown for each correlation. As we see in Table 2 and Fig. 3, model P1 is consistent within 2σ with the observed correlations between A2 maps and bright R6 sources (T3 and H3). We also see that these correlations are dominated by clusters of galaxies. On the other hand, the observed correlations between the bright source *removed* R6 map and the A2 maps are about a factor of 3 – 4 larger than the model predictions. In any case, the correlation is dominated by sources in the local universe ($z \lesssim 0.2$) and the expected correlation does not depend on the cosmological evolution significantly. The contribution of galactic stars, effects of minor modifications to the model, and the effects of possible extended components are discussed in the followings.

5.2. Contribution of Galactic Stars

Among the 835 serendipitously found X-ray sources in 780 deg^2 of high galactic latitude sky in the *Einstein* Extended Medium Sensitivity Survey (EMSS), about 25% are identified with galactic stars (Stocke et al. 1991). The identification was 96% complete and the flux limits of the survey range between $0.5 - 34 \times 10^{-13} \text{erg s}^{-1} \text{cm}^{-2}$ in the 0.3–3.5 keV band. When converted to the *ROSAT* R6 band, this corresponds to a flux range just below the detection limit in our source detection discussed in Sect. 3.2. Based on the flux-number ($\log N - \log S$) relation for the EMSS sample of stars, we have estimated the contribution of Galactic stars to the present correlation signals. Assuming a $kT = 2$ keV Raymond & Smith plasma spectrum with cosmic abundances, which is typical of a variable hard component of stellar coronal emission, the estimated

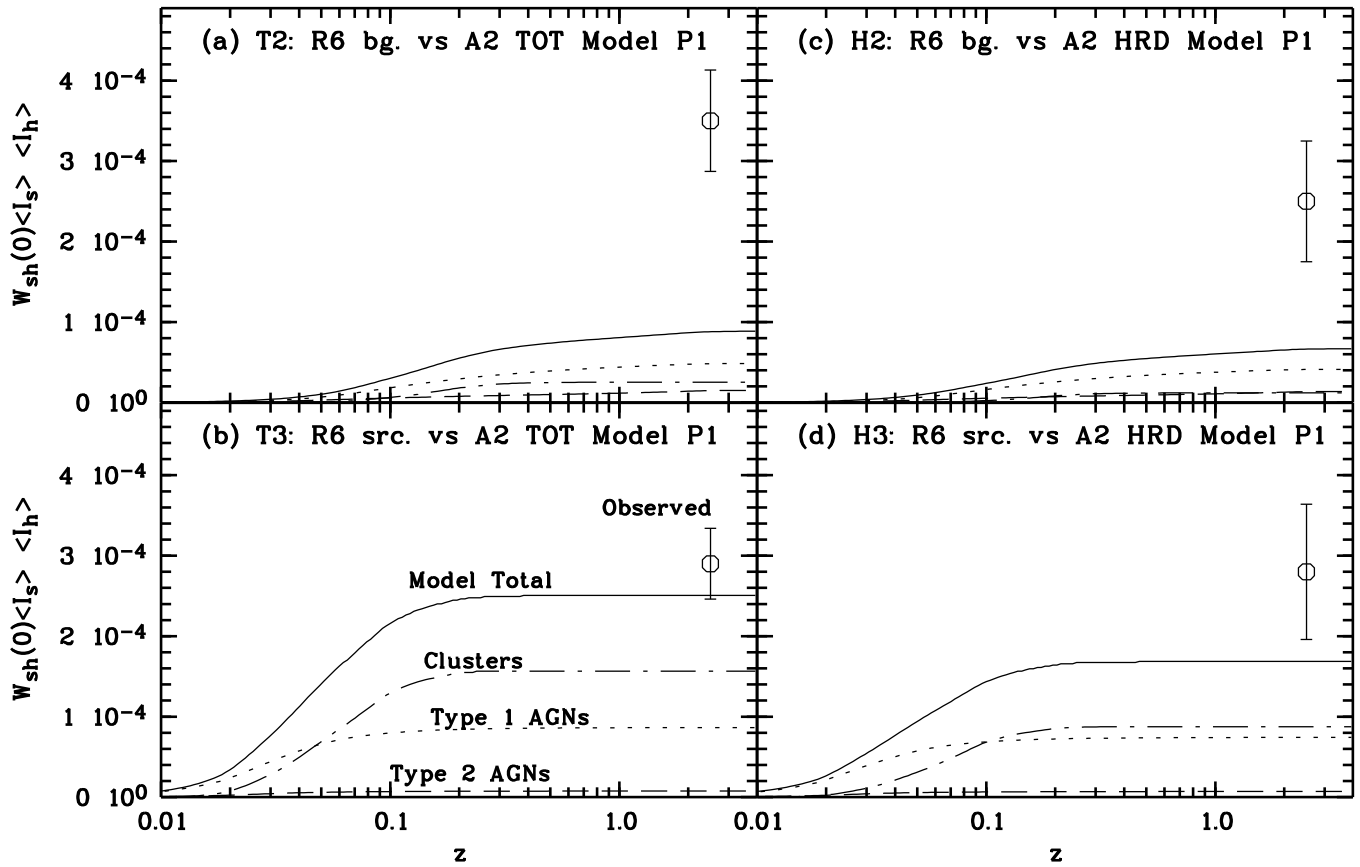


Fig. 3. The cumulative contributions of clusters, type 1 and 2 AGNs, and the total of these for model P1 to the observed CCFs are plotted. Each component is drawn in a different line style as labeled in the lower left panel. The observed values with 1σ error bars are also shown. The horizontal positioning of the observed data does not have any significance but placed there only for the convenience of the display.

contribution to the R6 background versus A2 TOT correlation (T2) is $\approx 3\%$ and R6 source versus A2 TOT correlation (T3) is $\approx 10\%$ of the observed. Thus, the contributions of galactic stars to the observed cross-correlations are within the statistical errors and not significant.

5.3. Unabsorbed Soft Component associated with AGNs

In our model P1, we used the AGN population synthesis model by Comastri et al. (1995). We here consider two minor modifications to this model. If a significant fraction of AGNs are embedded in groups of galaxies with X-ray emitting gas with $kT \sim 1$ keV, this could contribute to the soft-hard correlation. In many type 2 AGNs, there is an unabsorbed X-ray emitting component, which is believed to be electron-scattered X-rays from the nucleus. Comastri et al. (1995) et al. deliberately neglected this component because its luminosity is much weaker than the soft X-ray luminosity in type 1 AGNs with a comparable optical luminosity. We see the impact of these effects to our correlation.

In model P2, each AGN has an unabsorbed Raymond & Smith plasma component of $kT = 1$ keV with a 0.5 - 2 keV luminosity of $2 \times 10^{42} h_{50}^{-2} \text{ergs}^{-1}$. This is a typical value for most luminous groups of galaxies found in the *ROSAT* North Ecliptic Pole Survey (Henry et al. 1995). The spatial number density of groups of galaxies at this luminosity is several times $10^{-5} h_{50}^3 \text{Mpc}^{-3}$, which is comparable to the number density of Seyfert galaxies and about two orders of magnitude smaller than the number density of bright spiral galaxies. Thus, it is unlikely that every AGN is associated with a group of galaxies at this luminosity. The purpose of this model is not to be realistic but to examine the effect of the additional component. Table 2 shows that adding this component has little effect on the correlations T2 and H2, thus fails to explain the excess correlation even in this extreme case.

As another model, P3, we put a soft component to AGNs with fluxes proportional to the intrinsic (i.e. unabsorbed) luminosity. The underlying idea of this model, in terms of the unified scheme of AGNs, is to add an unabsorbed X-ray component in Seyfert 2, which is generally considered as electron-scattered nuclear emission.

Like Madau et al. (1994) considered in their model, we assume that 2% of the nuclear emission in type 2 AGNs are from the scattered component and can reach us without being absorbed. As we see in Table 2, this component is not sufficient to explain the observed excess correlation over model P1.

5.4. Low-Luminosity Flat X-ray Spectrum Galaxies

The Comastri et al. (1995) model deliberately neglected the contribution of low X-ray luminosity objects ($L_x \lesssim 10^{42} h_{50}^{-2} \text{erg s}^{-1}$) to the hard X-rays ($E \gtrsim 2 \text{ keV}$), while they left some room for these objects to contribute to soft X-rays ($E \lesssim 2 \text{ keV}$). However, Yaqoob et al. (1995) recently reported that NGC 3628, a low X-ray luminosity object, which had usually been classified as a starburst, has a rather flat X-ray spectrum (a photon index of $\alpha_{\text{ph}} = 1.2$). Based on this observation, they argued that a class of sources represented by this object could contribute significantly to the XRB. Here we estimate the contribution of the possible low luminosity population to our correlations. For an estimation, we consider low-luminosity X-ray galaxies of the 2 – 10 keV luminosity range of $10^{40} - 10^{42} h_{50}^{-2} \text{erg s}^{-1}$ at the present epoch. We assumed a power-law differential luminosity function ($d\Phi(L_x)/dL_x \propto L_x^{-\gamma}$) with $\gamma = 1$ and total 2 – 10 keV present-epoch volume emissivity of $2 \times 10^{38} h_{50} \text{erg s}^{-1} \text{Mpc}^{-3}$. This volume emissivity is an upper limit from the low-luminosity source contribution derived by Miyaji et al. (1994) based on the XRB- *IRAS* galaxy cross-correlation and has been considered in the Yaqoob et al. baseline model. For this population, we have assumed a power-law spectrum with $\alpha_{\text{ph}} = 1.2$ and simple luminosity evolution of $\propto (1+z)^{3.2}$ up to $z = 2$. The contribution of this population to our correlation calculated using above assumptions is only $\sim 1\%$ for either T2 or T3. Note that, in this model, most contribution to the correlation signal comes from around $z \sim 0.1$, unlike the contribution to the total surface brightness, which is mostly contributed from the high-redshift region given this evolution law. Thus this estimate is insensitive to the detailed behavior of the cosmological evolution. The above estimation shows that the low X-ray luminosity galaxies cannot explain the observed excess correlation in T2 or H2.

5.5. Extended Emission Component

We consider here the effect of the clustering term (or extended components) to the observed $W_{\text{sh}}(0)$. In the extragalactic component of the R6 (1 keV) map, Soltan et al. (1995) found a significant extended component in the auto-correlation function (ACF) at a scale of $\theta \lesssim 5^\circ$. They argued that the ACF signal they have found should be dominated by real extended structures rather than clustering of sources, based on comparison with the ACF in Soltan and Hasinger (1994) at smaller scales. They spec-

ulated that this component could be due to the clustering of groups of galaxies. However, information on statistical properties of groups of galaxies was very scarce and they did not make further arguments on this possibility.

The expected R6 ACF at $\sim 1^\circ - 3^\circ$ from the clusterings of AGN and clusters used in model P1 using Eq. 12 (in this case, two bands in the expression are the same) are two orders of magnitude smaller than the actual values observed by Soltan et al. (1995). We also checked if the AGN and cluster clusterings can explain the excess correlation in our zero-lag CCFs (T2 and H2). The expected clustering effects to the *ROSAT* – HEAO-1 zero-lag CCFs (because of the beam smearing, the zero-lag values are mainly due to the clustering at a scale of 1°) for the same model are also two orders of magnitude smaller than the observed excesses. For these estimates, we have assumed a form $\xi(r, z) = (r/r_0)^{-\gamma}(1+z)^{-3-\epsilon}$ for $r < 3r_0$ and $\xi(r, z) = 0$ for $r \geq 3r_0$. The parameters used for the estimations are $(r_0 [\text{km s}^{-1}], \gamma) = (1000, 1.8), (2400, 1.8)$ and $(880, 2.2)$ for the AGN-AGN, cluster-cluster (Bahcall 1988) and AGN-cluster (Lilje & Efstathiou 1988) correlation functions respectively. At the angular scales of degrees, the expected correlation is insensitive to the cosmological evolution of clustering and we have used $\epsilon = 0$. Since the discrepancies are two orders of magnitude, we also expect that the clustering of low X-ray luminosity objects (galaxies, low-luminosity AGNs), which have not been considered in the above calculation, cannot make much contribution, since their 2 – 10 keV X-ray volume emissivity should be lower than that of AGNs (Miyaji et al. 1994). Thus we expect that the Soltan et al.’s extended ACF component truly represents a new population of X-ray structure.

Here we consider a picture that the component responsible for the Soltan et al.’s ACF component is also responsible for the excess zero-lag CCF in T2 and H2. We constrain the nature of this component by comparing the upper-limit to our $\theta = 2.5^\circ$ CCF with their ACF and also investigate the contribution of this component to our zero-lag CCF. Since the spatial resolution of their ACF measurement is much higher than our CCF measurement, we have smoothed their ACF with the beam of our CCF (see Eq. [11]) and compared it with our CCF. The smallest angle where there is no overlap of the beams is at $\theta \sim 2.5^\circ$. At this angle, the smoothed ACF value is $\sim 1 \times 10^{-3}$, while the 2σ upper-limit of our CCF (T2) is 3×10^{-4} . Assuming that the detected R6 ACF is dominated by a single component with a single spectrum, the hard-to-soft flux ratio I_h/I_s of this component is:

$$(I_h/I_s) = (W_{\text{sh}}\langle I_h \rangle) / (W_{\text{ss}}\langle I_s \rangle). \quad (13)$$

The upper limit to this ratio is 1.3 (TOT cts s^{-1}) (R6 cts s^{-1}) $^{-1}$. This corresponds to a Raymond & Smith plasma with $kT \lesssim 2.5 \text{ keV}$ or a power-law photon index of $\alpha_{\text{ph}} \gtrsim 2.3$ for a galactic column density of $N_{\text{H}} = 1.8 \times 10^{20} \text{cm}^{-2}$.

Assuming that the structure causing the extragalactic 1 keV (R6) ACF in Soltan et al. (1995) in the $(0.1^\circ \lesssim \theta \lesssim$

3°) comes from a single extended component, we have calculated the expected zero-lag R6-A2 CCF ($W_{\text{sh}}(0)$). These values are shown under the models E1 (assuming a $kT = 2$ keV Raymond-Smith spectrum) and E2 ($kT = 1$ keV) (E represents the extended). A heavy metal abundance of 0.4 (cosmic) has been used in these estimations. Since the *ROSAT* R6 (1 keV) band is dominated by the Fe L emission lines, this estimate is sensitive to the heavy element abundance and should be taken as a rough measure.

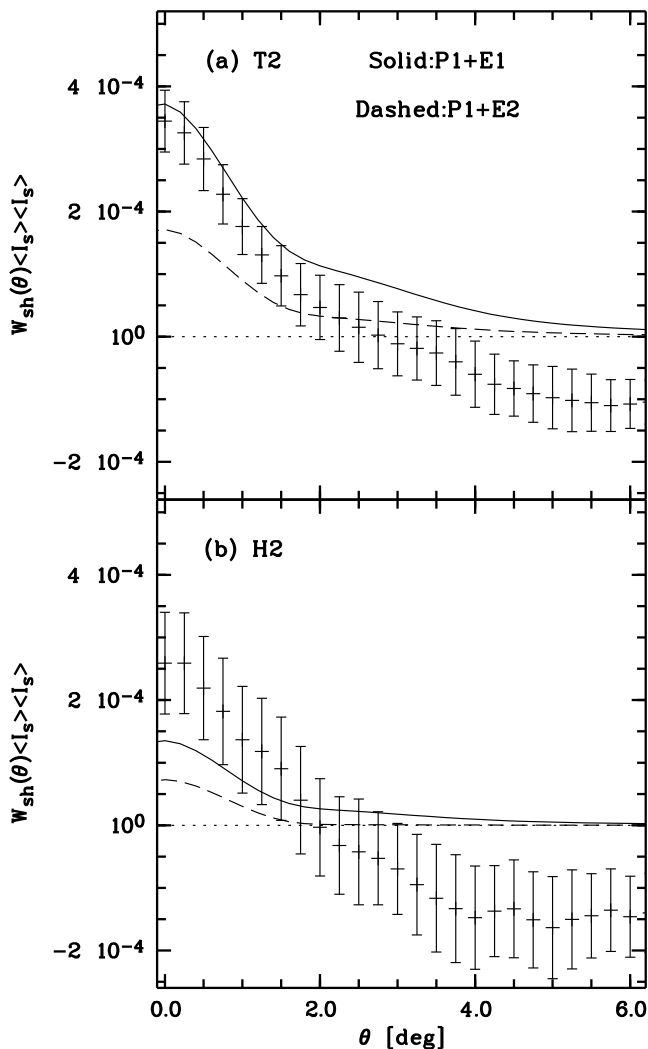


Fig. 4. The observed angular CCFs for the source-removed cases are shown with two models as indicated. The 1σ error bars are from the scatters in the ‘rotated’ correlations (dotted lines in Fig.2). Note that the errors in data points are not independent but highly correlated

Figure 4 shows the comparisons of the observed and modeled angular CCF for the source-removed cases. The models shown are E1 and E2 in addition to P1 as labeled. As we see in Fig. 4, model (P1+E1) could explain

the zero-lag amplitude of the CCFs. This means that if the extended component in the R6 ACF is a thermal plasma with $kT \sim 2$ keV this would also explain the excess zero-lag CCF over the model P1 prediction in our source-removed CCFs within 2σ . Considering that the H2 zero-lag correlation still exceeds the model P1+E1, while statistical significance is poor, a flatter spectrum in the $E \gtrsim 2$ keV range for this component is preferred. It is possible that the R6 ACF signal Soltan et al. (1995) found is composed of more than one component. For example, a composite model with a small-scale ($\theta \lesssim 2^\circ$) hard component and a large-scale ($2^\circ \lesssim \theta \lesssim 5^\circ$) soft component would better explain the data.

6. Concluding Discussions

As we see from the analysis presented above, AGNs and clusters account well for the correlation between the *ROSAT* bright R6 sources ($\gtrsim 0.08$ R6 cts s^{-1} , corresponds to 2.5×10^{-12} erg $\text{s}^{-1} \text{cm}^{-2}$) and the *HEAO-1* A2 surface brightness. This correlation is dominated by the Poisson effect from individual clusters of galaxies in the local universe. On the other hand, the correlations between the residual R6 background and the *HEAO-1* 1 A2 surface brightnesses are about a factor of 3 – 4 larger than the Poisson effect expected from the population synthesis model by Comastri et al. and clusters of galaxies based on the known X-ray luminosity functions. We have considered a few possible components which have not been considered in the population synthesis model, i.e., AGN-group association, unabsorbed (scattered) soft component in type 2 AGNs, and low-luminosity X-ray galaxies. Any of these three are not likely to explain the observed excess correlation.

Due to the large collimator beam of the *HEAO-1* A2 experiment, the zero-lag correlation could also be contributed by the clustering effect or an extended component. The extragalactic 1 keV (R6) angular auto-correlation function (ACF) by Soltan et al. (1995) clearly shows an extended structure up to a separation of several degrees. The origin of this component is not clear at this moment. They showed that the effects of rich clusters including the cluster-cluster clustering and the putative ~ 10 Mpc-scale diffuse gas component in their model only amounts to about one third of the R6 ACF signal. They suggested diffuse emission from groups of galaxies could possibly contribute to the R6 ACF. However, statistical properties concerning poor groups, e.g. luminosity/temperature functions and clustering properties with rich clusters/AGNs, are scarcely known. Comparing the 1 keV ACF with the upper-limit to our R6 – A2 (TOT) CCF at $\theta = 2.5^\circ$, the minimum angular separation where beams do not overlap, we have constrained the spectrum of the extended structure causing this R6 ACF signal. This corresponds to a Raymond & Smith plasma of $kT \lesssim 2.5$ keV

or a power-law photon index of $\alpha_{ph} \gtrsim 2.3$. Suppose the component responsible for the 1 keV ACF has a spectrum with an 'equivalent color-temperature' of $kT \sim 2$ keV, this component explains the correlation in excess of the population synthesis model expectation, assuming that the extended R6 ACF structure is composed of a single component. A picture where there are a harder small-scale component and a softer large-scale component would better explain the data.

There remains also a possibility that some major change to the Comastri et al. population synthesis model or an introduction of a new population is needed, while the extended component has a lower temperature (or a steeper spectrum). The current observation cannot discriminate between these two, since it is limited by the low spatial resolution of the *HEAO-1* A2 experiment. A large area survey at $E \gtrsim 2$ keV with higher spatial resolution in a future mission such as *ABRIXAS* (Friedrich et al. 1996) would enable us to discriminate between these two pictures. With an analysis similar to that presented here, but with a higher spatial resolution, we can constrain the spectrum of the extended component and give another crucial observational constraint to the population synthesis models simultaneously.

Acknowledgements. TM is supported by a fellowship from the Max-Planck Society. TM appreciates the hospitality of the Astrophysikalisches Institut Potsdam during his visit. The authors thank Keith Jahoda for his help in handling the *HEAO-1* A2 data and Elihu Boldt for encouragements. This work has made use of data from two X-ray satellites, *ROSAT* and *HEAO-1*, in orbit about a decade apart from each other. The authors appreciate the effort of all people which lead to the success of these two missions. Thanks are also due to the referee, Luigi Danese, for useful comments and suggestions.

References

- Allen J., Jahoda K., & Whitlock, L. 1994, *Legacy* 5, 27
- Awaki H., Koyama K., Inoue H., & Halpern J.P. 1991, *PASJ* 43, 195
- Bahcall N.A. 1988, *ARA&A* 26, 631
- Barcons X., Branduardi-Raymont G., Warwick, R.S., Fabian, A.C., Mason K. O., McHardy I., & Rowan-Robinson M., 1994, *MNRAS*, 268, 833
- Barcons X., Franceschini A., Danese L., De Zotti G. & Miyaji T. 1995 *ApJ*, 455, 480
- Boyle B.J., Griffiths R.E., Shanks T., Stewart G.C. & Georgantopoulos I. 1993, *MNRAS* 260, 49
- Boyle B.J., Shanks T., Georgantopoulos I., Stewart, G.C., & Griffiths, R.E. 1994, *MNRAS* 271, 639
- Carrera F.J. et al. 1991, *MNRAS* 249, 698
- Comastri A., Setti G., Zamorani G., & Hasinger G. 1995, *A&A* 296, 1
- Danese L., Toffolatti L., Franceschini A., Martín-Mirónes J.M., & De Zotti G. 1993, *ApJ*, 412, 56
- David L. P., Slyz A., Jones C., Forman W., Vrtilik S. D., & Arnaud, K. A. 1993, *ApJ* 412, 479
- Edge A. C., Stewart G. C., Fabian A. C., & Arnaud K. A. 1990, *MNRAS* 245, 559
- Friedrich P. et al. 1996, in *Röntgenstrahlung from the Universe*, eds. Zimmermann H.U. & Trümper J., MPE report, in press
- Gioia I.M., Maccacaro T., Schild R.E., Wolter A., Stocke J.T., Morris S.L. & Henry J.P. 1990, *ApJS*, 72, 567
- Hasinger G., Burg R., Giacconi R., Hartner G., Schmidt M., Trümper J., & Zamorani G. 1993, *A&A* 275, 1
- Henry J.P. et al. 1992, *ApJ* 386, 408
- Henry J.P. et al. 1995, *ApJ* 449, 422
- Jahoda K. 1993, *Adv. Space Res.* 13, No.12, 231
- Jahoda K., Lahav O., Mushotzky R., Boldt E. 1991, *ApJ* 378, L37
- . 1992, *ApJ* 399, L107 (Erratum)
- Lahav O. et al. 1993, *Nature* 364, 693
- Lilje P.J. & Efstathiou G. 1988, *MNRAS* 231, 635
- Madau P., Ghisellini G. & Fabian A.C. 1994, *MNRAS* 270, L17
- Miyaji T. 1994, PhD Thesis, University of Maryland
- Miyaji T., Lahav O., Jahoda K., & Boldt E., 1994, *ApJ* 434, 424
- Mulchaey J.S., Mushotzky, R.F., & Weaver, K.A. 1992 *ApJ* 390, L69
- Pfeffermann, E. et al. 1986, *Proc SPIE* 733, 519
- Piccinotti G. et al. 1982, *ApJ* 253, 485
- Roche N., Shanks, T., Georgantopoulos, I., Boyle B.J., & Griffiths, R.E. 1995, *MNRAS* 273, L15
- Rothschild R.E. et al. 1979, *Sp. Sci. Instr.*, 4, 269
- Schartel N., Schmidt M., Fink H. H., Hasinger G., & Trümper J. 1995, preprint
- Shafer R. A. 1983 PhD Thesis, University of Maryland
- Soltan A. & Hasinger G. 1994, *A&A* 288, 77
- Soltan A., Hasinger G., Egger R., Snowden S., & Trümper J. 1995, *A&A*, in press
- Snowden S.L. & Schmitt, J.H.M.M. 1990, *Ap&SS*, 171, 207
- Snowden S.L., McCammon D., Burrows D.N., Mendenhall J.A. 1994, *ApJ* 424, 714
- Snowden S.L. et al. 1995, *ApJ* in press
- Stocke J.T., Morris S.L., Gioia I.M., Maccacaro T., Schild R., Wolter A., Fleming T.A., & Henry, J.P. 1991, *ApJS* 76, 813
- Trümper J. *Adv. Space Res.* 2, No.4, 241
- Voges W. 1992, in *Proceedings of Satellite Symposium 3, Space Science with particular emphasis on High-Energy Astrophysics*, ed. T.D. Guyenne & J.J. Hunt (noordwijk:ESA Publication Division), 9
- Voges W. 1995, private communication
- Yaqoob T., Serlemitsos P.J., Ptak, A., Mushotzky R., Kunieda H., & Terashima Y. 1995, *ApJ*, 455, 508
- Zimmermann H.U., Becker W., Belloni T., Döbereiner S., Izzo, C., Kahabka P. & Schwentker O. 1994, *EXSAS User's Guide*, MPE Report 257, Garching